CONSTITUTIVE RESPONSE OF RENÉ 80 UNDER THERMAL MECHANICAL LOADS

K.S. Kim, T.S. Cook, R.L. McKnight
General Electric Company
Cincinnati, Ohio 45215

Accurate prediction of structural response in the high temperature environment is a prerequisite for reliable life prediction of hot section components of gas turbine engines. In many situations, this involves the use of general purpose finite element code capable of modeling nonlinear material behavior. The constitutive models of material behavior may be either classical, i.e. separation of creep and plastic deformation, or unified, wherein inelastic deformation as a whole is considered. While there is considerable interest in the unified theories, these models require further development of capabilities and experimental verification under realistic loading conditions. At present, the implementation of unified theories in numerical analysis is not widespread. The classical theories, on the other hand, are relatively well established and available in many finite element codes. Therefore, the prediction of cyclic deformation in this study was made using a classical model rather than a unified theory. The objective of the study was to examine the accuracy of a classical constitutive model when applied to thermomechanical fatigue (TMF) of Rene' 80. Using isothermal creep and cyclic stress-strain data, two approaches were used to predict the half life thermal mechanical hysteresis loops. An elastic-plastic analysis using appropriate stress-strain-rate data was followed by an elastic-plastic-creep analysis. This latter approach used high strain rate data for the elastic-plastic analysis and relied on the explicit inclusion of creep to develop the appropriate time dependent behavior. Comparison of the two approaches provides an indication of the importance of explicitly modeling the rate effects in the thermal mechanical cycles of Rene' 80.

MATERIAL

The material selected for this study is the conventionally cast superalloy Rene' 80. The composition (wt. pct.) is: 3.0 pct. Al, 5.0 pct. Ti, 14.0 pct. Cr, 3.9 pct. W, 4.0 pct. Mo, 9.8 pct. Co, 0.17 pct. C, and the balance Ni. This nickel-base material is a typical high temperature alloy and is quite widely used for turbine blades and nozzle vanes. The microstructure of this alloy has been described by Antolovich and Domas [1,2], but it consists of large (ASTM 2 to 3), irregular grains with a distribution of grain boundary carbides and borides. There are several strengthening mechanisms but the major one is uniformly distributed cuboidal gamma prime precipitates. These precipitates tend to coarsen with increasing temperature and strain rate and are at least partially responsible for the temperature dependence of cyclic deformation. At the lowest test temperature, the deformation is largely within the matrix leading to matrix failure when a critical dislocation density is achieved. At the higher temperatures, the large precipitates tend to disperse the slip, yielding more homogeneous deformation. The damage accumulates at grain boundaries, leading to the formation of oxide spikes [1]; hence, not only the deformation but also the failure mechanisms are temperature dependent.

MECHANICAL TESTING

Solid cylindrical specimens were cast to size and final machined using low stress procedures. The specimens had a diameter of 6.35mm and were 92.1mm in length. The specimen ends were threaded for attachment purposes.

A broad sequence of thermomechanical and isothermal tests were carried out to develop and evaluate a TMF model. Isothermal cyclic stress-strain (CSS), low cycle fatigue (LCF), creep, and relaxation tests were conducted at three temperatures under a variety of test conditions. The CSS behavior was examined as a function of strain rate, as was the LCF life. Creep and relaxation were examined in tension and compression; mean stress effects and creep-plasticity interactions were investigated. All these results will not be reported here; this paper will concentrate on the time dependent behavior of Rene' 80.

All testing was carried out in conventional servohydraulic fatigue machines with extensometry. For the displacement controlled tests, total longitudinal strain was controlled. The same test setup was used for the creep tests so that the creep curve was obtained. Data were obtained at three temperatures, 760, 871, and 982°C; the majority of the testing was done at the highest temperature. Cyclic testing was done at strain rates of 10, 2, and 1 percent/minute, with a few tests at 0.2 percent/minute. Previous testing had established stress-strain behavior at high strain rates, 40-50%/min. [2,3]. Triangular waveforms were used in these tests with several strain ratios ($R_\varepsilon = \varepsilon_{min}/\varepsilon_{max}$) employed.

The cyclic stress-strain data was obtained in two ways. At a strain rate of one percent/minute, fully reversed cyclic tests with open hysteresis loops were conducted. By recording the loops, the material's approach to stable behavior was observed. A loop at the estimated half life was selected as representative of the cyclic amplitude curve. Other strain rate data was obtained from the LCF tests; the stress-strain values at 0.5 N_f were taken as points on the cyclic curve. A summary of the cyclic behavior at the three temperatures and four strain rates is shown in Figure 1. The data shows a complex pattern of temperature dependent behavior. At 760C, there is very little effect of strain rate. At 871C, the strength shows a significant increase with rate, while the 982C stress-strain curve increases only at the very high rate. This behavior reflects the temperature dependent deformation mechanism of Rene' 80.

Since the TMF cycles had a period of less than three minutes, the creep tests concentrated on the early part of the creep curve. The stress levels employed were typical of the TMF loads and the initial load was applied at approximately the rate of the TMF tests. There was slight plasticity in a few cases but most of the initial loading was elastic. The majority of the creep tests lasted two to three hours, although a few were taken to failure.

The creep data was analyzed using a nonlinear regression routine and fitted with the creep curve

$$\varepsilon^c = K\,\sigma^m t^n + Q\,\sigma^r t \quad , \tag{1}$$

where K, m, n, Q, and r are constants determined by the regression.

Both the tensile and compressive creep data were analyzed using this expression. It was found that the compression curves could be reasonably predicted by the tensile data and vice versa. In addition, when the creep rates were examined, at 982C (the only temperature examined at present), the same creep rates were occurring at the same creep strain regardless of the sign of the load. Figure 2 shows the tensile creep data and the resulting curve fits at 982 and 871C. Since there does not appear to be any variation in creep associated with the sign of the load, this same fit was used to describe both the tensile and compressive creep in the modeling.

The Rene' 80 TMF specimens were subjected to the three temperature and strain waveforms shown in Figure 3. The general testing procedure has been described by Embley and Russell [4] and consists of two control loops, one for strain and one for temperature. Induction heating was employed and controlled by calibrated thermocouples mounted on the specimen shoulders. The TMF cycle was limited by the solid specimens; forced air cooling would induce undesirable temperature gradients and was not employed. A strain rate of one percent per minute was used in the TMF experiments; this resulted in a period of 1.6 to 2.6 minutes. This consideration restricted the temperature cycle to 100-150^{o}C. This cycle is, of course, not representative of an entire flight cycle, but it does simulate parts of the cycle, for example, a thrust reversal [5].

Load-displacement hysteresis loops were recorded periodically throughout the TMF and LCF tests. Load and strain data were recorded on calibrated strip charts and used to determine cycles to crack initiation, N_i, and failure, N_f. The Rene' 80 softened at a constant rate for much of the fatigue test; an acceleration in the softening rate was used to define crack initiation. Cycles to failure was defined as 50 percent load drop. The hysteresis loop nearest $N_f/2$ was used as the definition of cyclic values. Stress values and strain ranges were obtained from this loop. The measured plastic strain range was defined as the maximum width of the stress-strain hysteresis loop.

THERMAL MECHANICAL ANALYSIS

Analyses of the thermal mechanical hysteresis loops were made using the four constant strain triangle model shown in Figure 4. The finite element program developed by McKnight [6] was used throughout the study. Two approaches were taken to account for the inelastic deformation at high temperatures. In the first approach, only the elastic and plastic deformation was considered. The creep was not explicitly included in the analysis. Instead, the stress-strain curves at the strain rate used in the TMF tests were input to the analysis. It may be assumed that the creep was implicitly included in this case since the creep effects are reflected in the rate-dependent stress-strain curves.

In the second approach, the creep deformation was explicitly included. The stress-strain curves at high strain rates, 50%/min, along with creep constants, were input to the analysis. It was assumed that the creep deformation is negligible at the high strain rate. All the stress-strain curves used as input in the analysis are half-life curves, as are the hysteresis loops being calculated in this paper. From the standpoint of life prediction, using half life data is more practical than relying on the data based on continuous changes of cyclic response, which is difficult to predict for the classical constitutive models.

The thermal mechanical cycles analyzed in this study are (Figure 3):

(i) 760 - 871°C, R_ε = -1, $\Delta\varepsilon$= 1%, $\dot{\varepsilon}$ = 1%/min; LIP, CWD, LOP
(ii) 871 - 982°C, R_ε = -1, $\Delta\varepsilon$= 1%, $\dot{\varepsilon}$ = 1%/min; LIP, CWD, LOP

For comparison purposes, isothermal cycles are also presented:

(iii) 871°C, R_ε = -1, $\Delta\varepsilon$= 1.0%, $\dot{\varepsilon}$ = 2%/min
(iv) 982°C, R_ε = -1, $\Delta\varepsilon$= 1.3%, $\dot{\varepsilon}$ = 2%/min and 10%/min

For the elastic-plastic analysis, the six cycles in (i) and (ii) were analyzed. For elastic-plastic-creep analysis, conditions (ii), (iii) and (iv) were considered. The 760-871^{o}C cycles were not considered in the latter approach because the creep tests were completed only for 871^{o}F and 982^{o}C at this time.

For completeness of presentation, the constitutive model used herein is outlined in the following:

(I) Time-Independent Deformation

The strain component can be written as the sum of the elastic, plastic and thermal parts:

$$\varepsilon_{ij} = \varepsilon^{e}_{ij} + \varepsilon^{p}_{ij} + \varepsilon^{\theta}_{ij} \quad . \tag{2}$$

The elastic and thermal strains are given by:

$$\varepsilon^{e}_{ij} = \frac{1+\nu}{E}\,\sigma_{ij} - \frac{\nu}{E}\,\delta_{ij}\,\sigma_{kk} \quad , \tag{3}$$

$$\varepsilon^{\theta}_{ij} = \alpha\delta_{ij}\Delta T \quad , \tag{4}$$

where E is the Young's modulus, ν is the Poisson ratio, α is the thermal expansion coefficient, δ_{ij} is the Kronecker delta and ΔT is the relative temperature. For the plastic deformation, the classical incremental plasticity theory which utilizes the Prandtl-Reuss flow rule, Von Mises yield criteria and the kinematic hardening rule in the strain space, has been used in this study. The Besseling's subvolume method [7] is used within this constitutive framework. In the subvolume method a strain-hardening material is considered as a composition of several subvolumes, each of which is an elastic-ideally plastic material. The subvolumes have identical elastic constants but different yield stresses. The yield function for the k-th subvolume is given by

$$f_k = (e_{ij} - e^{p}_{ijk})\ (e_{ij} - e^{p}_{ijk}) - P_k^{\,2} \quad , \tag{5}$$

where e_{ij} is the strain deviator, e^p_{ijk} is the plastic component of e_{ij} for the k-th subvolume and P_k is the radius of the k-th subvolume yield surface ($P_1 < P_2 < \ldots$). Notice that the kinematic hardening rule in the strain space is used in Eq. (5). The plastic deformation for each subvolume is assumed to be isochoric, i.e., $\dot{\varepsilon}_{iik}=0$, which implies $\dot{\varepsilon}^p_{ijk}=\dot{e}^p_{ijk}$. The plastic strain rate of the k-th subvolume is given by

$$\dot{e}^p_{ijk} = \frac{(e_{ijk} - e^p_{ijk})\,(e_{mn} - e^p_{mnk})\,\dot{e}_{mn}}{P_k^2} \quad , \tag{6a}$$

if

$$f_k = 0 \text{ and } (e_{ij} - e^p_{ijk})\,\dot{e}_{ij} > 0$$

and

$$\dot{e}^p_{ijk} = 0 \quad , \text{otherwise.} \tag{6b}$$

The total plastic strain can be written as the weighted sum of the plastic strains of the subvolumes satisfying Eq. (6a):

$$\dot{e}^p_{ij} = \sum_k \Psi_k \; e^p_{ijk} \tag{7}$$

The determination of Ψ_k, and also P_k in Eq. (5), can be done by considering the uniaxial stress-strain curves. For details, the reader is referred to Besseling [7].

The elastic properties and the stress-strain curves are input at several temperatures. In a time-varying temperature field, for example, the thermomechanical process under consideration, the material data, E, ν, α, P_k and Ψ_k, are linearly interpolated using the input data at nearest temperatures.

(II) Time-Dependent Deformation

The total strain in the presence of creep is given by

$$\varepsilon_{ij} = \varepsilon^{e}_{ij} + \varepsilon^{p}_{ij} + \varepsilon^{c}_{ij} + \varepsilon^{\theta}_{ij} \quad , \tag{8}$$

where ε^{c}_{ij} is the creep strain and others are as given in equation (2). The creep strain components are given by

$$\dot{\varepsilon}^{c}_{ij} = \lambda S_{ij} \tag{9}$$

where S_{ij} is the stress deviator, λ is a function of the history of creep deformation. Defining $\dot{\bar{\varepsilon}}^{c}$ such that

$$\dot{\bar{\varepsilon}}^{c} = \sqrt{\frac{2}{3} \dot{\varepsilon}^{c}_{ij} \dot{\varepsilon}^{c}_{ij}} \tag{10}$$

it can be shown that

$$\lambda = \frac{3}{2} \frac{\dot{\bar{\varepsilon}}^{c}}{\bar{\sigma}} \tag{11}$$

where

$$\bar{\sigma} = \sqrt{\frac{3}{2} S_{ij} S_{ij}} \tag{12}$$

The constancy of the volume in creep deformation $\dot{\varepsilon}^c_{kk} = 0$, is again assumed here. The effective creep strain, $\bar{\varepsilon}^c$, is determined by the primary creep term of the Bailey-Norton type and a steady state creep term;

$$\bar{\varepsilon}^c = K \bar{\sigma}^m t^n + Q \bar{\sigma}^r t \quad , \tag{13}$$

where the constants are those from (1) and

$$\bar{\varepsilon}^c = \int_0^t \dot{\bar{\varepsilon}}^c \, dt \quad . \tag{14}$$

Differentiating (13) with respect to time and using equations (9), (11) and (12), one can show that

$$\dot{\varepsilon}^c_{ij} = \frac{3}{2} S_{ij} K n \bar{\sigma}^{m-1} t^{n-1} \tag{15}$$

for small times where the primary creep dominates. In terms of accumulated creep strain, equation (15) can be written as

$$\dot{\varepsilon}^c_{ij} = \frac{3}{2} S_{ij} K^{\frac{1}{n}} n \bar{\sigma}^{\frac{m}{n}-1} (\bar{\varepsilon}^c)^{1-\frac{1}{n}} \tag{16}$$

Equation (15) is called "the time-hardening formulation" and equation (16) is called the "strain-hardening formulation" in the context of the creep analysis under time-varying stress field. In this study, the strain-hardening formulation was used simply because it is somewhat favored over the time-hardening relation from the standpoint of correlating test data. In the case where the steady state creep is not negligible, the creep time for a given creep strain must be determined numerically. Then, the creep strain rate is determined from Eq. (15) with an additional term for the steady state creep. In this study, the secondary creep was included even though the primary creep was dominant.

The stress reversal was assumed to occur if

$$(\varepsilon_{ij}^{c} - \varepsilon_{ij}^{*})\,\sigma_{ij} < 0 \qquad (17)$$

where ε_{ij}^{*} is the strain origin which is updated, if necessary, after each stress reversal. Further explanation of the stress reversal and also the algorithm of application of the strain-hardening rule can be found in Kraus [8].

In the finite element analysis, the creep constants K, m, n, Q, and r are input at a number of temperatures. The creep constants at an intermediate temperature are linearly interpolated using the data at nearest temperatures.

DISCUSSION OF RESULTS

(I) Elastic-Plastic Analysis

The stress-strain curves at the 1%/min strain rate which were input to the analysis are shown in Figure 1. Note in the figure that the strain rate effects below the rate of 10%/min are rather small at 982°C, but they were considerably larger at 871°C. The analysis results obtained are shown in Figures 5 and 6 for 760-871°C in-phase and 871-982°C 90° out-of-phase cycles, respectively. The point "P" on the curves designates the point where plasticity develops. For further details of the results, the reader is referred to Cook, et al. [9]. In general, the agreement between the computed and the experimental hysteresis loops was very good. In particular, excellent correlation between analysis and test results was found for 871-982°C cycles for all three phases. The 760-871°C results were satisfactory but not as good as the 871-982°C results. This could reflect the changing inelastic deformation mechanisms over the 760-871°C temperature range as discussed by Antolovich, et al. [1,10]. It should be possible to improve the correlation by incorporating more stress-strain curves between the two temperatures. Unfortunately, such data are unavailable at this time.

(II) Elastic-Plastic-Creep Analysis

The material data base for this model, the high strain rate CSS curves and the creep curves, are those in Figures 1 and 2. Using these data, the elastic-plastic-creep analysis modeled the cycle using linear strain ramps; the cycle was divided into 38 identical time steps. For each step, the elastic-plastic stress analysis was done for the strain increment; then the stress was relaxed in the strain hold over the time increment. The average values of the stress in the strain hold were used in the hysteresis loop plots. The maximum stress relaxation in a step was approximately 70 MPa. The temperature in the strain hold was set equal to the temperature at the midpoint of the time step.

First, the isothermal temperature hysteresis loops were obtained at 2%/min and 10%/min strain rates. The 2%/min hysteresis loops at 871^{o}C and 982^{o}C are shown in Figures 7 and 8. The correlation between prediction and observation is excellent for both temperatures.

The 871-982^{o}C thermal mechanical cycles were reanalyzed for the three phases. The hysteresis loops are presented in Figures 9, 10 and 11 and are compared to the experimental curves and the elastic-plastic results. The shapes of the hysteresis loops agree very well; in particular note the flattening of the loops in the region of the maximum temperature. The general features of the CWD loop are accurately reproduced but note that the loop bears more resemblance to the in-phase than the out-of-phase cycle. This qualitative observation is supported by the TMF life prediction model work of Reference 9. That investigation showed that, in terms of life modeling, the CWD cycle was similar to the LIP cycle and the same stress/temperature parameters could be used in both.

A comparison of the three 871-982C cycles predicted by the elastic-plastic and elastic-plastic-creep models shows that there is not much difference in the results of the two models. The elastic-plastic model is marginally better at predicting the hysteresis loop of the CWD cycle but the results are quite

similar for the other two cycles. The plastic strain range agreement is excellent; the time dependence of the load shows some variation among the two models and the experimental results. The discrepancies in hysteresis loop prediction seem to be associated with temperature increasing from 871 to 982C and indicate too high a strength level in this regime. It has not been determined whether this is due to the material data or the constitutive model itself. It must be pointed out that the predicted versus observed loops were not as good for the lower temperature cycle, 760-871^{o}C, in Reference 9. The generation of creep data at 760C is presently underway and it will be very interesting to see whether the inclusion of explicit time dependence improves the prediction. The results for this one temperature cycle suggest that the use of high strain rate and creep data can produce hysteretic behavior that is nearly as good as an analysis based on the correct strain rate.

CONCLUSIONS

This paper examines the applicability of a classical constitutive model for stress-strain analysis of a nickel-base superalloy, Rene' 80, in the gas turbine TMF environment. A variety of tests were conducted to generate basic material data and to investigate the material response under cyclic thermomechanical loading. Isothermal stress-strain data were acquired at a variety of strain rates over the TMF temperature range. Creep curves were also generated over the same temperature regime. Three TMF cycles were examined at two temperature ranges, 871-982C and 760-871C. Only the former temperature cycle was modeled in this paper as some of the 760C creep data had to be regenerated.

Two approaches were taken to analytically predict the hysteresis loops. In the first approach, the elastic-plastic deformation was considered with rate-dependent stress-strain curves. In the second approach, the creep deformation was explicitly included and the stress-strain curves at high strain rates were input to the analysis. The results indicate that both approaches provide accurate hysteretic behavior of Rene' 80 under the TMF loading. The correlation of the predicted and observed hysteresis loops was excellent over 871-982^{o}C for all three cycles using both approaches. The

elastic-plastic model predictions did not compare with experiment as well for the temperature range 760-871^{o}C [9]. As soon as the appropriate data is available, this cycle will be examined with the elastic-plastic creep model. For the cycles examined, either model approach can be employed depending on the material data available.

The results of this paper provide optimism on the ability of the classical constitutive model for high temperature applications, at least for the material under consideration. Further efforts with wider range of temperature cycles and more general loading, including the effects of hold time, mean stress and strain, would be worthwhile.

REFERENCES

1. Antolovich, S. D., Domas, P. A., and Strudel, J. L., Met. Trans. A, 10A, December 1979, pp. 1859-1868.

2. Domas, P. A., "An Investigation of Notch Low Cycle Fatigue Life Behavior of Rene' 80 at High Temperature," Ph.D. Dissertation, University of Cincinnati, 1981.

3. Miller, M. A., Unpublished Research, General Electric Aircraft Engine Group, Cincinnati, Ohio.

4. Embley, G. T. and Russell, E. S., Proceedings of the First Parsons International Turbine Conference, Institute of Mechanical Engineers, 1984, p. 157.

5. McKnight, R. L., Laflen, J. H., and Spamer, G. T., "Turbine Blade Tip Durability Analysis," NASA Report 165268, National Aeronautics and Space Administration, February 1982.

6. McKnight, R. L., "Finite Element Cyclic Thermoplasticity Analysis by the Method of Subvolumes," Ph.D. Dissertation, Department of Aerospace Engineering, University of Cincinnati, 1975.

7. Besseling, J. F., "A Theory of Plastic Flow for Anisotropic Hardening in Plastic Deformation of an Initially Isotropic Material," Report S. 410, National Aeronautical Research Institute, Amsterdam, 1953.

8. Kraus, H., Creep Analysis, Wiley-Interscience, 1980, Chapter 2.

9. Cook, T. S., Kim, K. S., McKnight, R. L., "Thermal Mechanical Fatigue of Cast Rene' 80," presented at the ASTM Symposium on Low Cycle Fatigue - Directions for the Future, 30 Sept.-4 Oct., 1985, Lake George, N.Y., In Press.

10. Antolovich, S. D., Baur, R., and Liu, S., in Superalloys 1980, J. K. Tien, et al. eds, ASM, 1980, pp. 605-613.

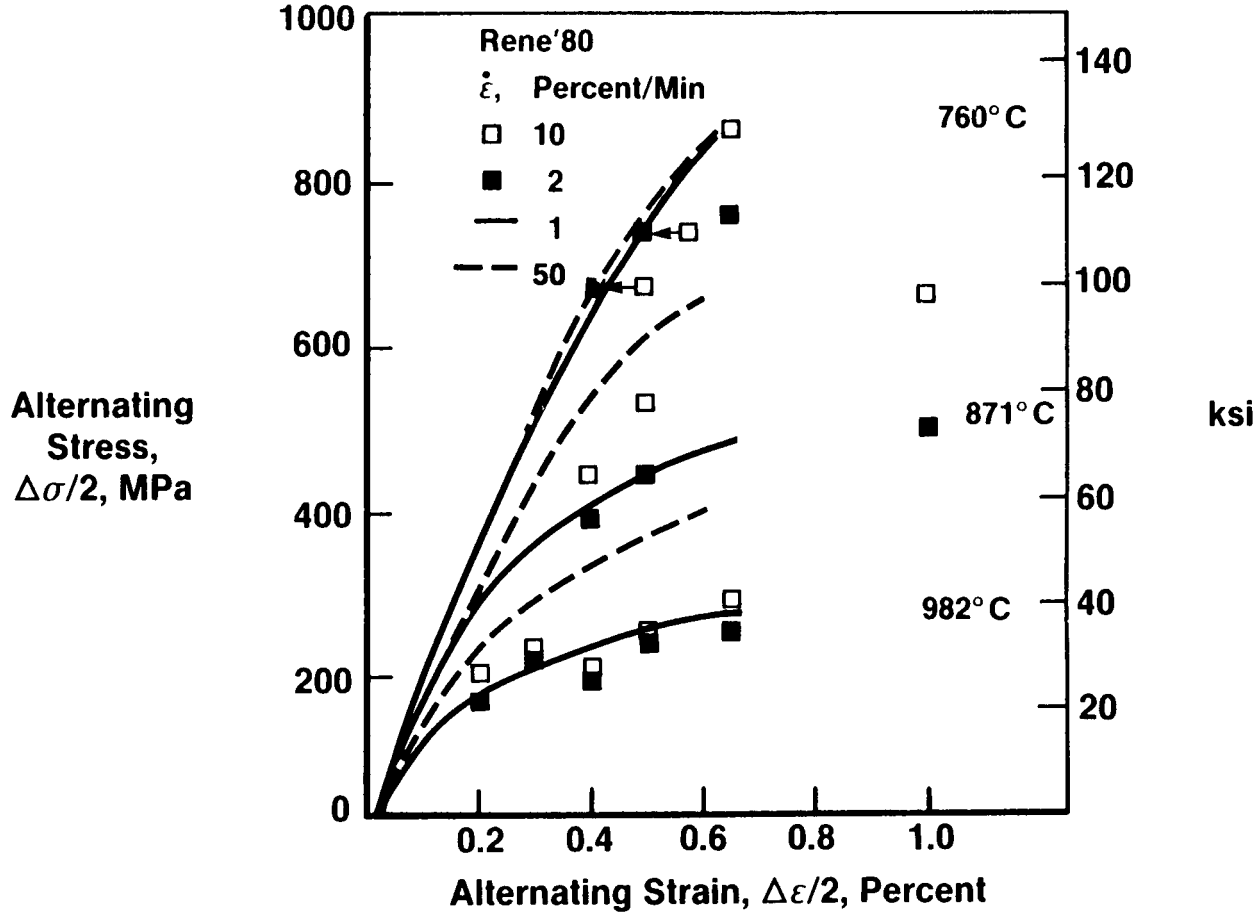

Figure 1. - Cyclic Stress-Strain Behavior for Rene' 80

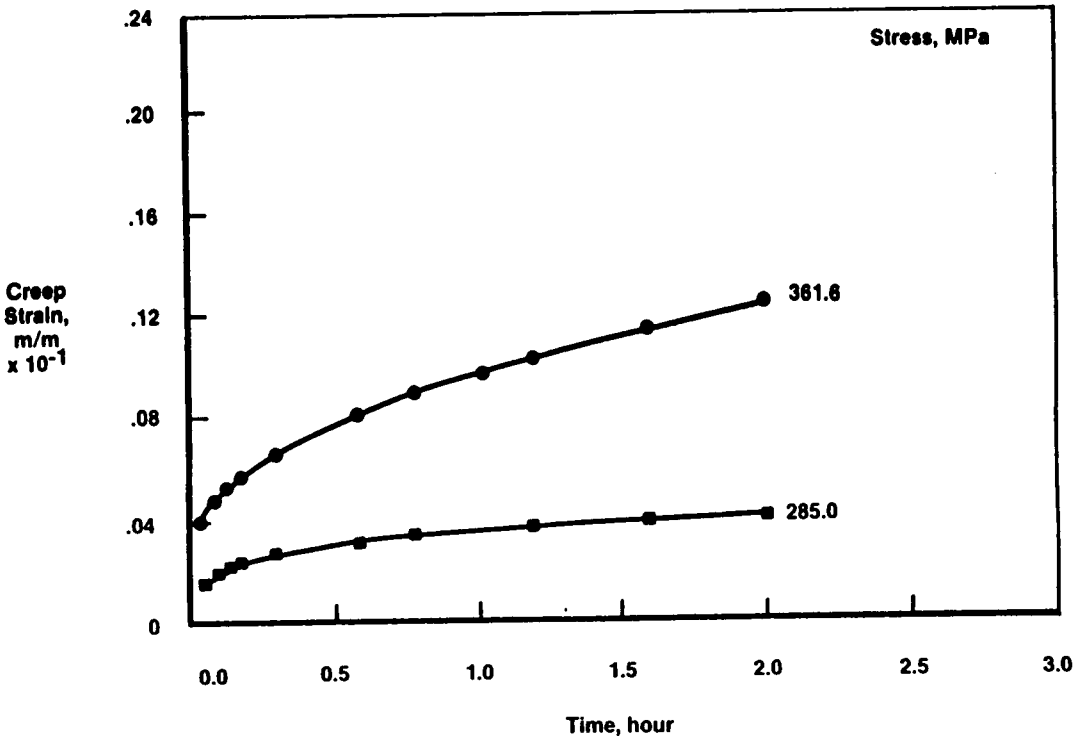

Figure 2a. - Creep Data and Curve Fits at 871°C

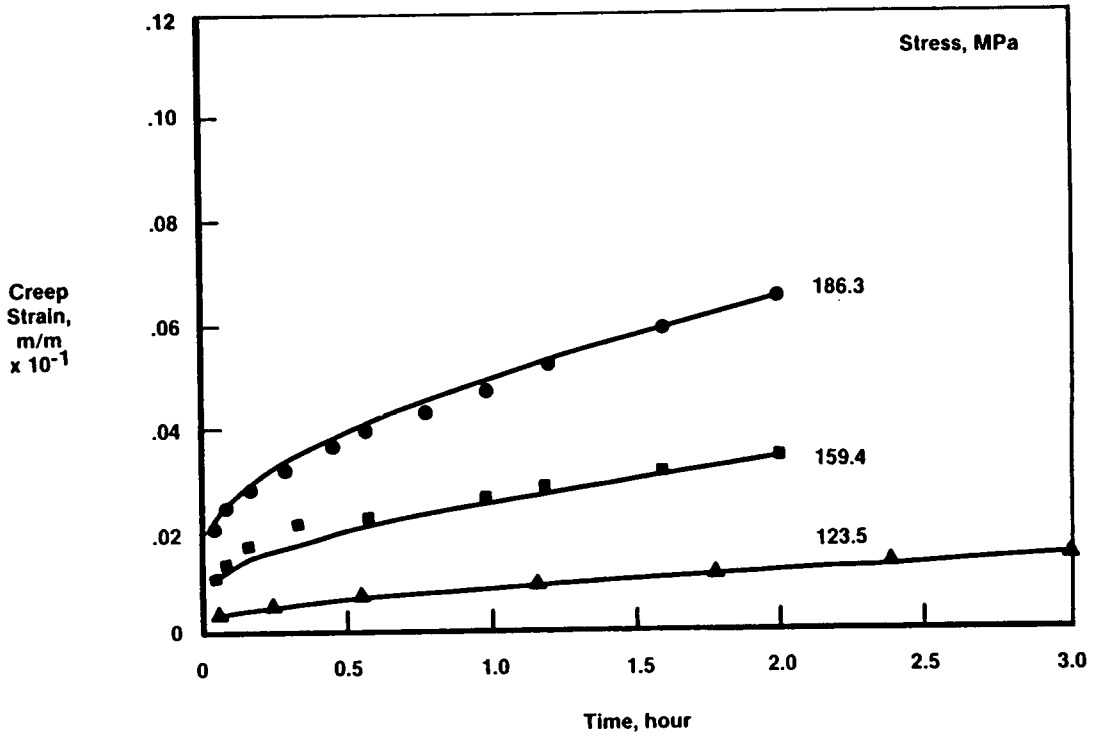

Figure 2b. - Creep Data and Curve Fits at 982°C

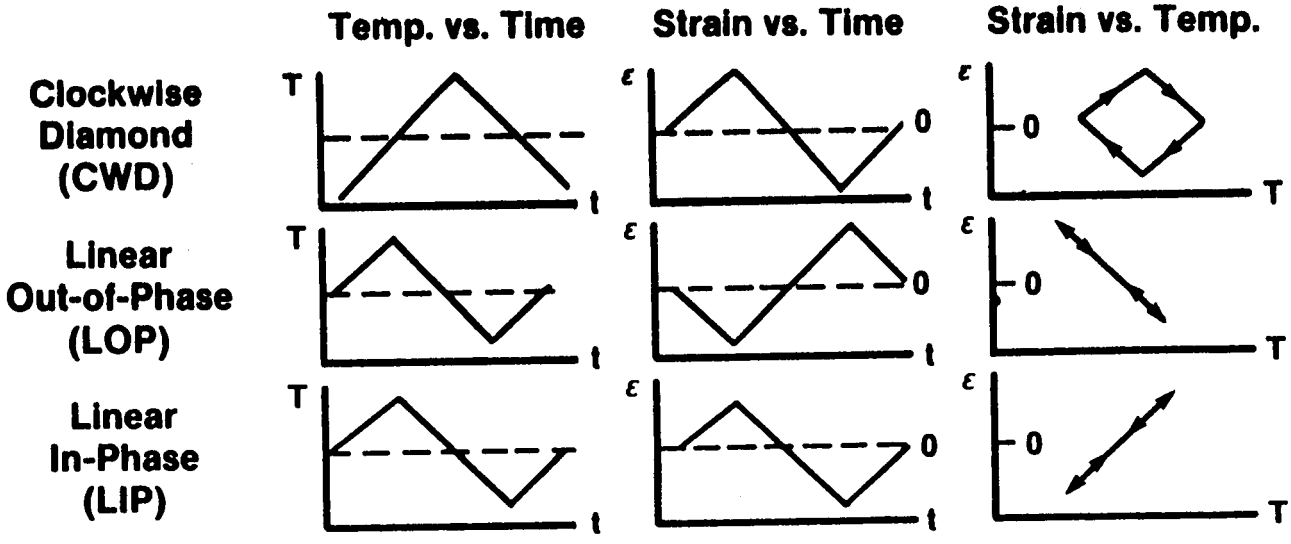

Figure 3. - Thermal Mechanical Cycles Examined in the Investigation

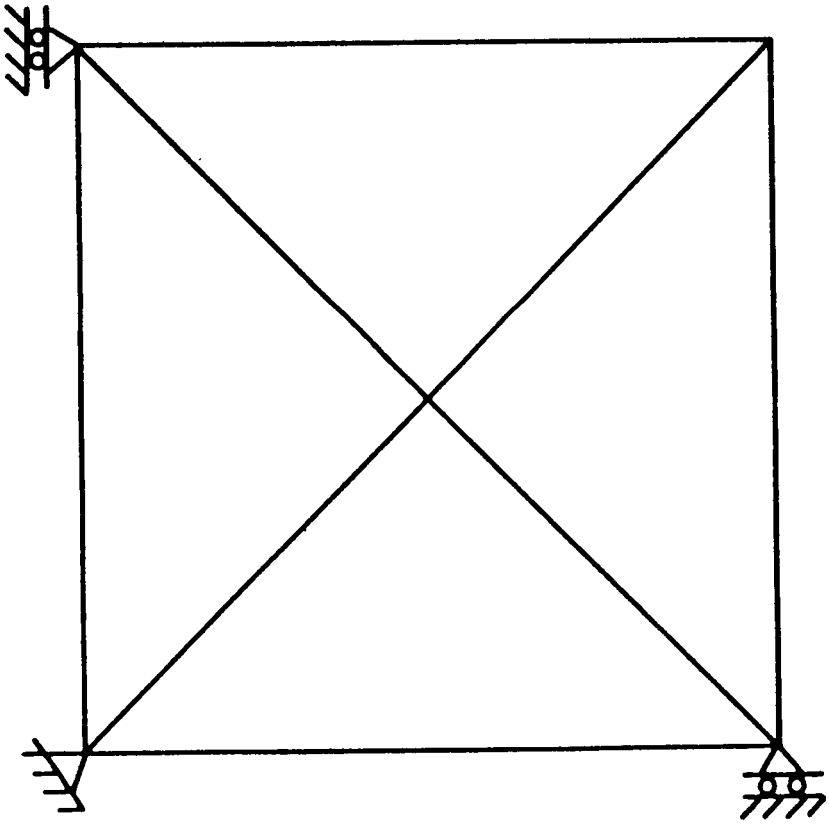

Figure 4. - Finite Element Model Used in TMF Modeling

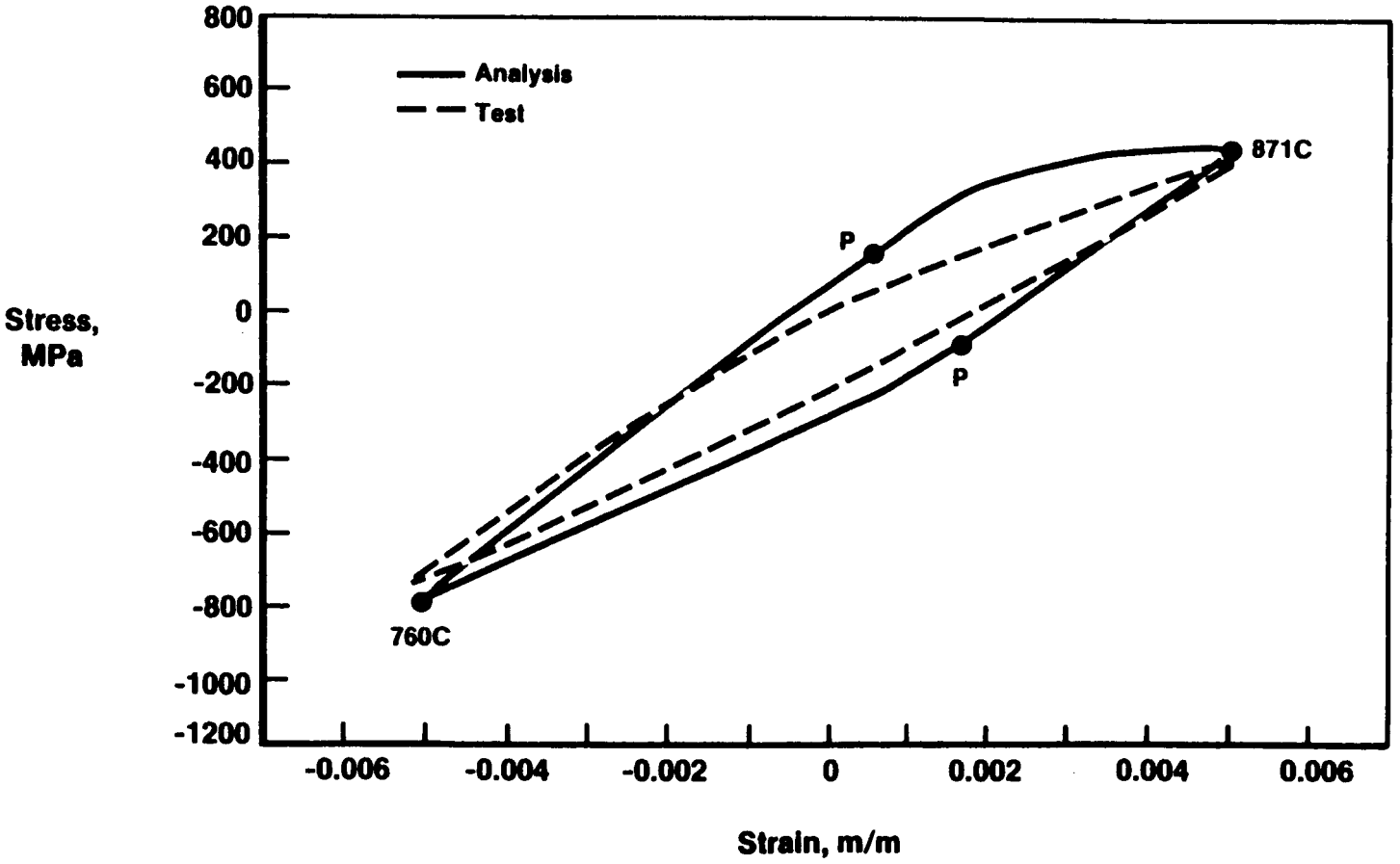

Figure 5. - Predicted Vs. Observed Constitutive Behavior, 760-871^{o}C LIP TMF Cycle, Elastic-Plastic Analysis

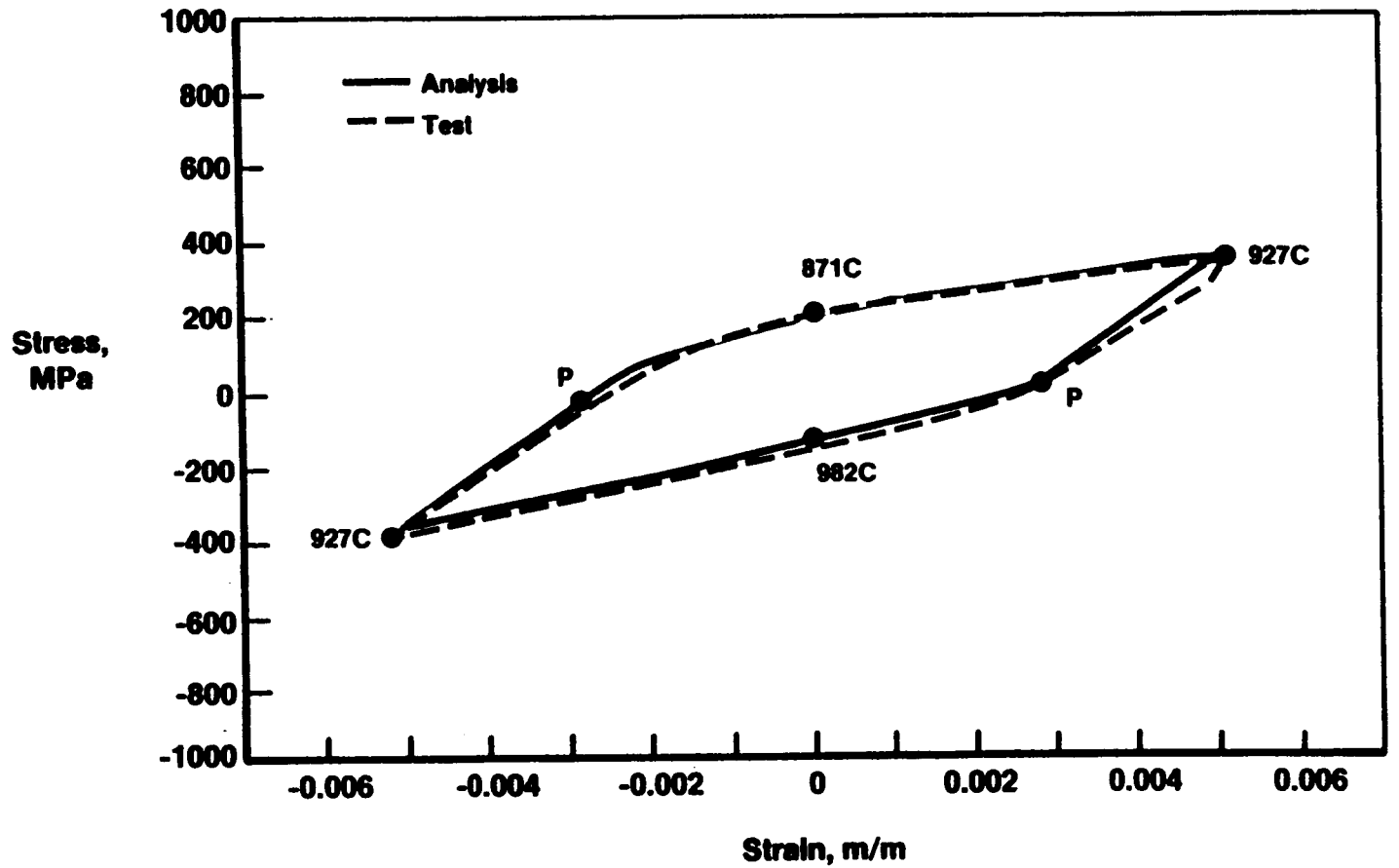

Figure 6. - Predicted Vs. Observed Constitutive Behavior 871-982°C CWD TMF Cycle, Elastic-Plastic Analysis

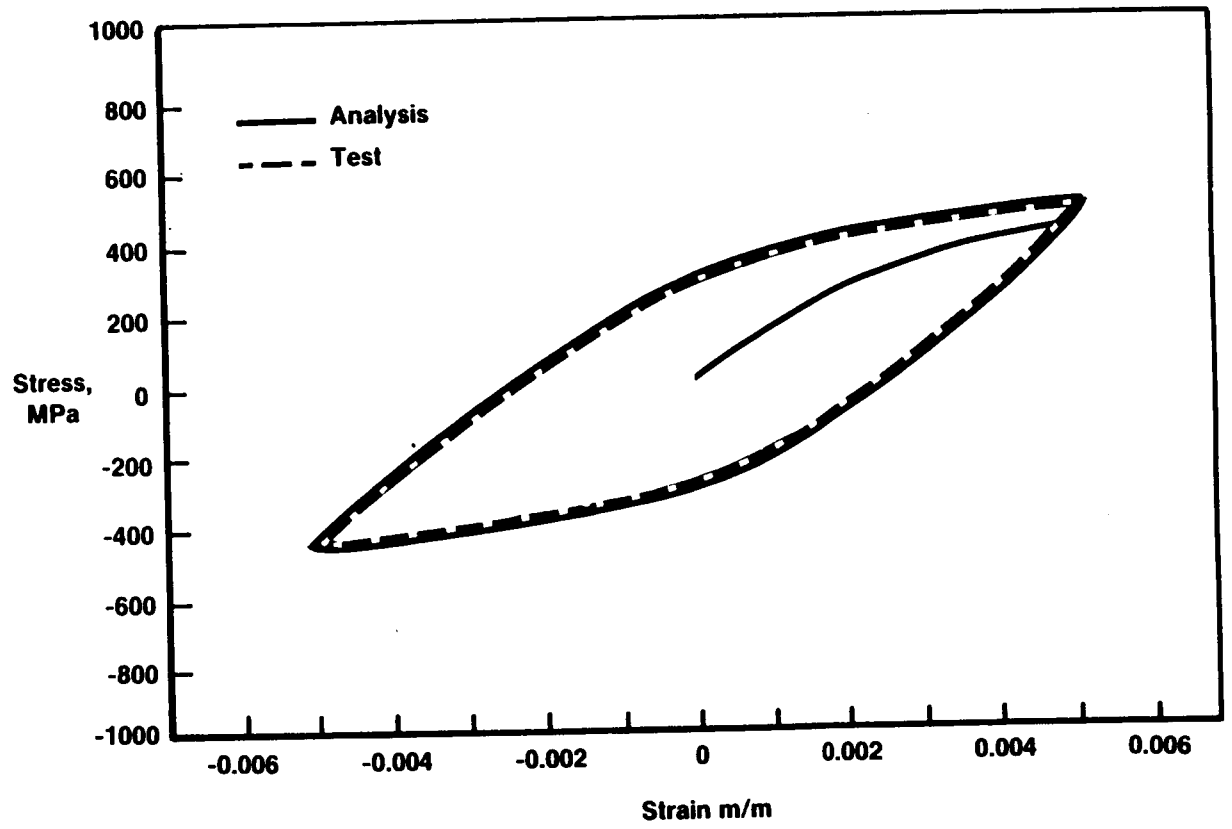

Figure 7. - Predicted Vs. Observed Constitutive Behavior, 871^{o}C, 2%/min, Elastic-Plastic-Creep-Analysis

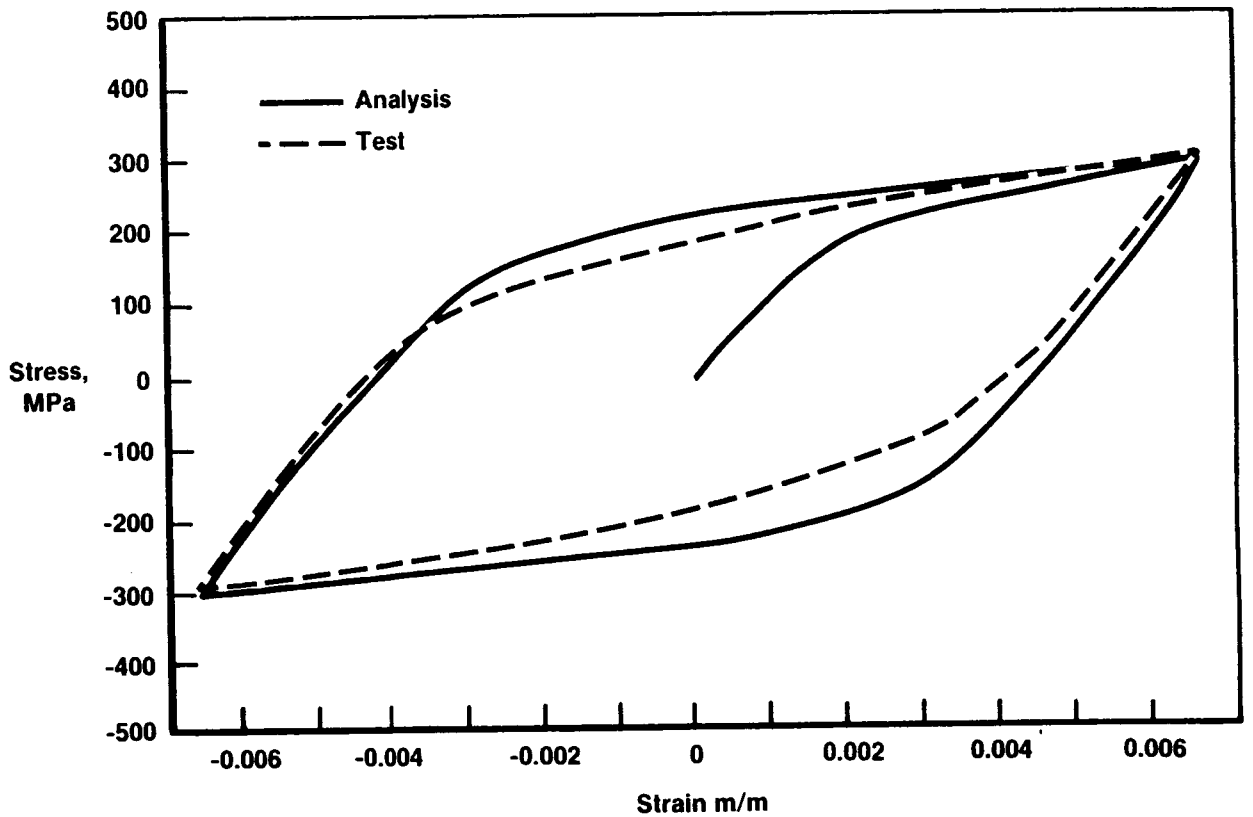

Figure 8. - Predicted Vs. Observed Constitutive Behavior, 982^{o}F, 2%/min, Elastic-Plastic-Creep-Analysis

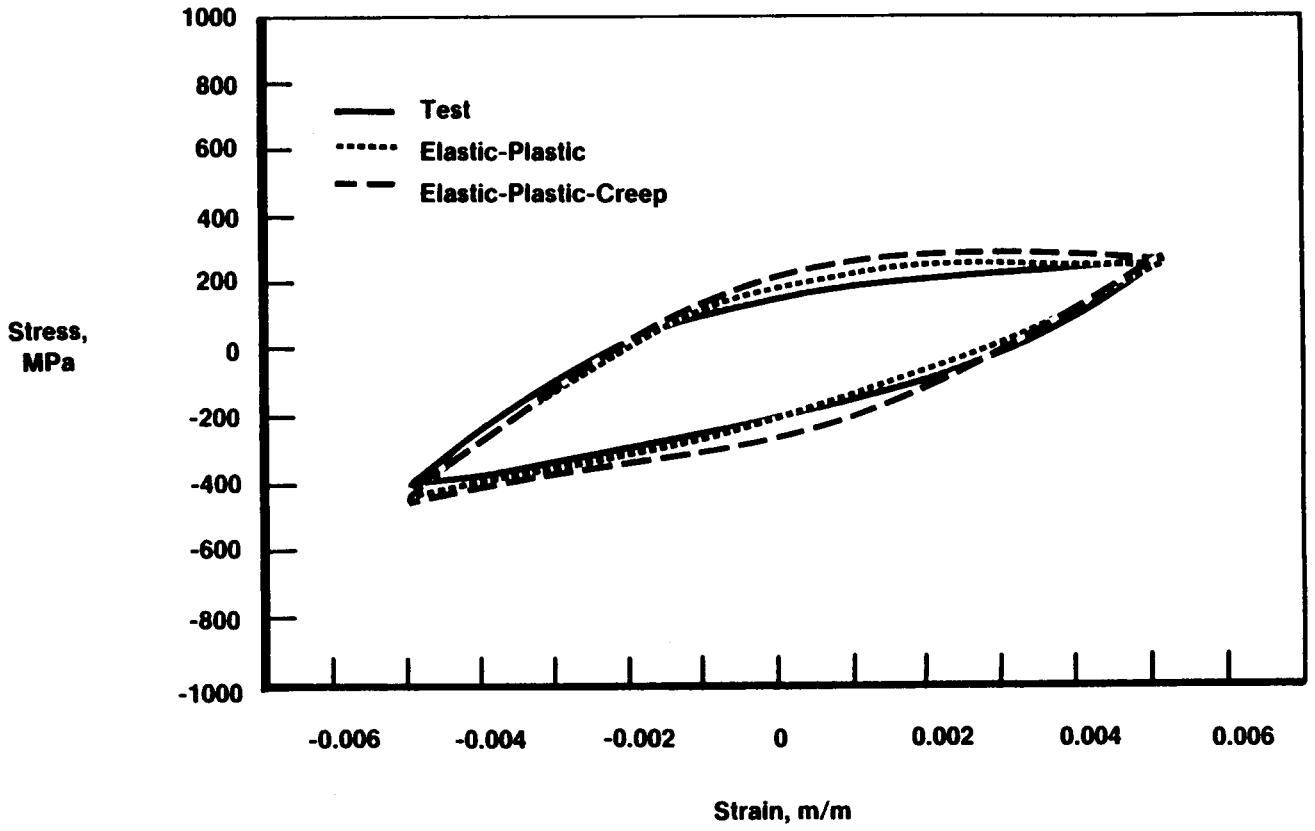

Figure 9. -Predicted Vs. Observed Constitutive Behavior, 871-982^{o}C, LIP TMF Cycle, Elastic-Plastic-Creep and Elastic-Plastic Analysis

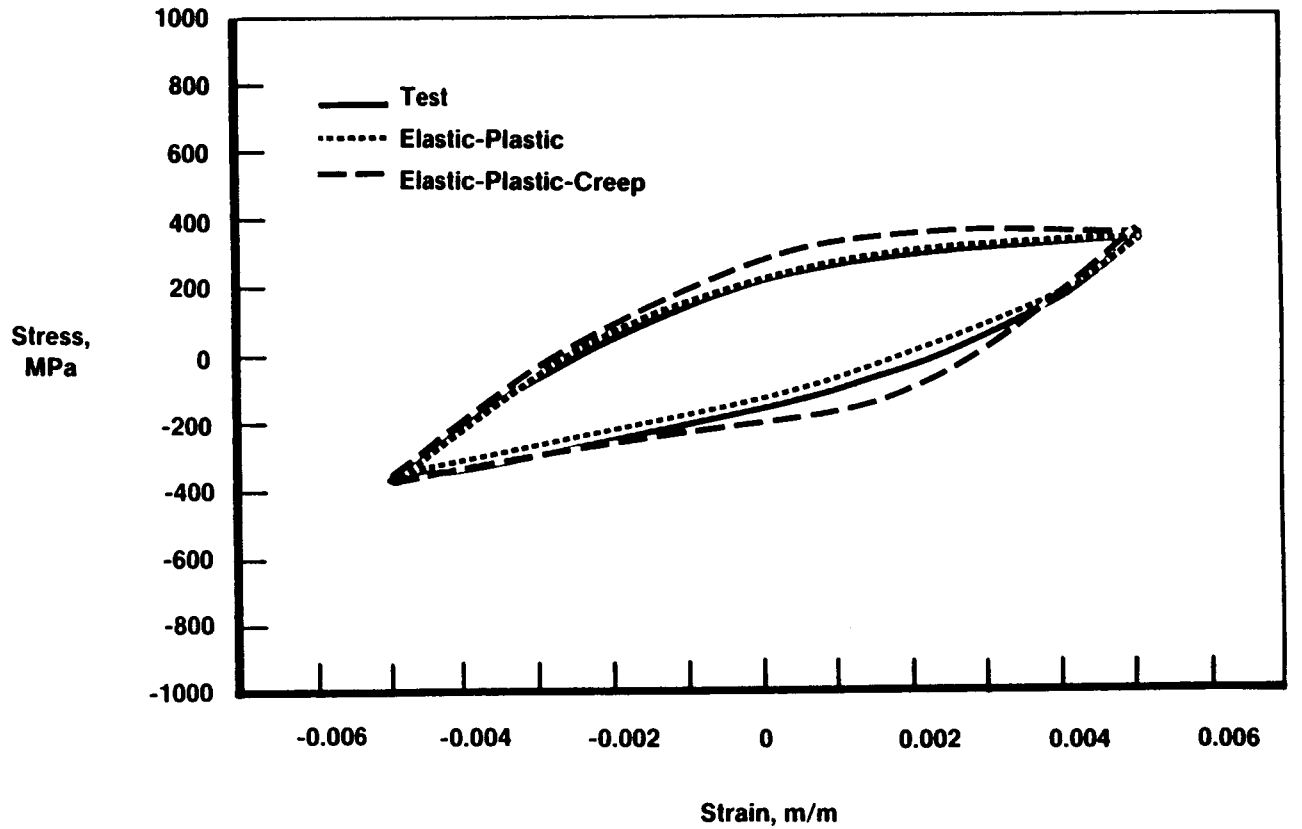

Figure 10. - Predicted Vs. Observed Constitutive Behavior, 871-982°C, CWD TMF Cycle, Elastic-Plastic-Creep and Elastic-Plastic Analysis

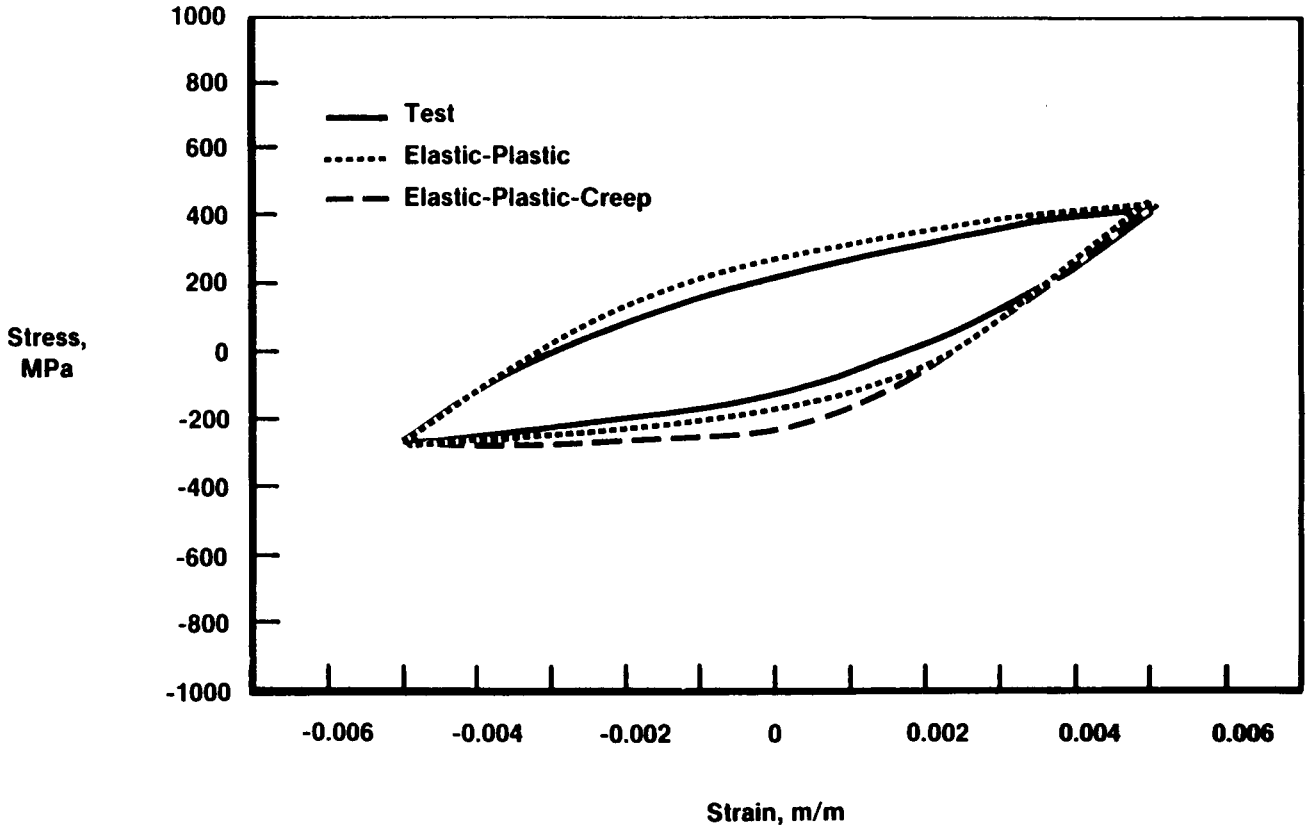

Figure 11. -Predicted Vs. Observed Constitutive Behavior, 871-982°C, LOP TMF Cycle, Elastic-Plastic-Creep and Elastic-Plastic Analysis